2025 IEEE INTERNATIONAL WORKSHOP ON MACHINE LEARNING FOR SIGNAL PROCESSING, AUG. 31– SEP. 3, 2025, ISTANBUL, TURKEY

THE SAMPLING-ASSISTED PATHLOSS RADIO MAP PREDICTION COMPETITION

Çağkan Yapar[‖,*] *Stefanos Bakirtzis*[‖,$,†] *Andra Lutu*[‡]
Ian Wassell[†] Jie Zhang[§,#] Giuseppe Caire[*]

[*]Technical University of Berlin, [†]University of Cambridge
[‡]Telefonica Research, [§]University of Sheffield, [#]Ranplan Wireless

ABSTRACT

To encourage further research and facilitate fair comparisons of deep learning–based pathloss estimation methods in indoor environments, particularly in the less-explored case of having access to sparse ground truth pathloss samples in tandem with physical propagation environment information, we organized the MLSP 2025 Sampling-Assisted Pathloss Radio Map Prediction Data Competition. This overview paper describes the sampling-assisted indoor pathloss prediction problem, the datasets used, the competition tasks, and the evaluation methodology. Lastly, it provides an overview of the submitted methods and the results of the challenge.

***Index Terms*—** Radio map, pathloss, deep learning, challenge, dataset.

1. INTRODUCTION

In wireless communications, pathloss (PL)—also referred to as the large-scale fading coefficient—is a metric that quantifies the attenuation of signal strength between a transmitter (Tx) and a receiver (Rx) due to large-scale effects. These effects include free-space propagation loss, and interactions such as penetration, reflection, and diffraction of radio waves with objects and structures in the propagation environment. A wide range of existing and emerging applications in wireless communications are inherently dependent on the precise location-specific knowledge of PL, the so-called PL radio maps. Consequently, reliable estimates of this quantity are essential. A non-exhaustive list of indicative use cases includes: user-cell site association, network deployment, fingerprint-based localization, physical-layer security, optimal power control, path planning, and activity detection [1].

The estimation of PL and other wireless channel characteristics can be achieved through the utilization of radio propagation models. Existing channel modeling techniques exhibit a notorious trade-off. Deterministic models, such as ray tracing, are highly accurate when precise physical information about the propagation environment is available, namely the geometry and electromagnetic material properties of the environment's objects and structures. However, these models are computationally demanding. The opposite is true for empirical and stochastic models. They are not computationally demanding, but their accuracy is low. Recently, considerable effort has been made to develop data-driven methods that can be trained to yield commensurate accuracy with deterministic propagation models. These methods, which utilize the same physical environment information as the deterministic models, exhibit impressive computational efficiency due to the native graphics processing unit (GPU) parallelization of deep neural networks (DNNs) [2] (see e.g. [3, 4, 5] and the surveys [6, 1, 7, 8] for the specific case of PL estimation considered in this competition). In contrast to the outdoor scenarios, where reflected and diffracted electromagnetic field components dominate, in indoor environments, refracted field components through obstacles play a more significant role. Furthermore, the accurate estimation of indoor radio maps necessitates the consideration of the diverse range of construction materials and their electromagnetic properties [4].

This work aspires to promote further research and enable fair comparisons of DNN-based indoor PL estimation methods, particularly in the less studied scenario where sparse ground truth PL samples along with detailed environment information are available. To this end, inspired by the success of the *First Pathloss Radio Map Prediction Challenge at ICASSP 2023* [9, 1] and the *First Indoor Pathloss Radio Map Prediction Challenge at ICASSP 2025* [10], we released an indoor PL radio map dataset generated via ray tracing simulations and organized the *Sampling-Assisted Pathloss Radio Map Prediction Data Competition at MLSP 2025*.[1]

The challenge consisted of two tasks focused on predicting PL radio maps using deep learning (DL)-based methods, leveraging sparse ground truth PL samples collected at varying sampling rates from the propagation environment (see, e.g., [3, 11]). The first task involved a uniform, random selection of ground truth PL sampling locations. The second

[‖]These authors contributed equally to this work.

[$]Stefanos Bakirtzis' work is supported by the EPSRC IAA Strategic Impact Partnership Fund and the Foundation for Education and European Culture.

[1]https://sapradiomapchallenge.github.io

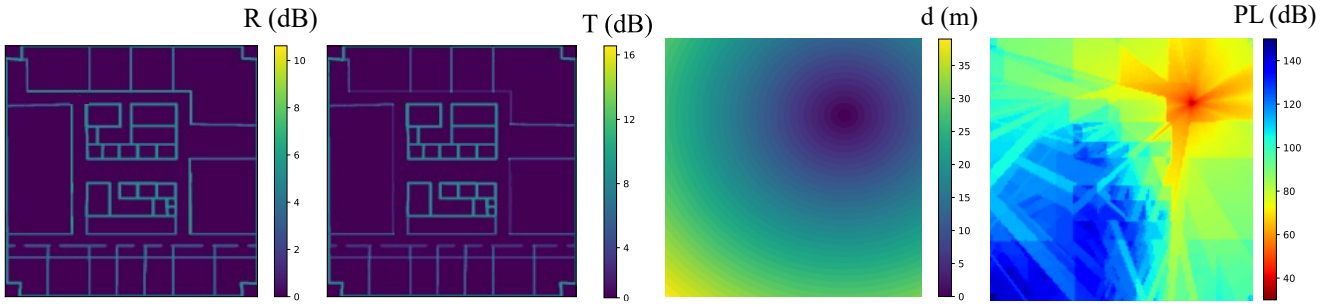

(a) Reflection coefficient (b) Transmission coefficient (c) Distance input (d) Target PL radio map

Fig. 1: An example from the Indoor Radio Map Dataset: **(a)-(c)** the three channels of the RGB input image; **(a)** the normal incidence reflectance and **(b)** transmittance coefficients at each point of the grid, **(c)** the distance between Tx and each point; **(d)** the target PL radio map.

task investigated how sampling location selection impacts radio map estimation accuracy, exploring efficient techniques beyond random sampling.

Remark 1: *To prevent potential confusion, it should be emphasized that the competition setting was still based on training on a large dataset in a fully supervised manner, where all the PL values in the target radio maps are available. The sparse samples from the ground truth radio maps should be considered an additional source of information, in addition to the physical information about the propagation environment.*

2. DATASET - THE INDOOR RADIO MAP DATASET

The *Indoor Radio Map Dataset* that we previously made public [12] includes various indoor PL radio maps generated using *Ranplan Wireless* [2] ray tracing software in different settings. For this competition, a subset of the dataset was used.

2.1. Training Dataset

For the current data competition, the Task 2 sub-dataset of the Indoor Radio Map Dataset was designated as the training dataset. This sub-dataset includes PL radio maps from 25 indoor environments of various sizes, and complexity, comprising different construction material types (e.g., concrete, plasterboard, wood, glass, and metal), 50 randomly assigned isotropic Tx positions per indoor layout, and 3 Tx signal frequency bands (868 MHz, 1.8 GHz, and 3.5 GHz), amounting to a total of 3750 radio maps.

For all ray tracing simulations, both the Tx and receiving plane were set at a height of 1.5 meters above the floor. The spatial resolution was set to 0.25 m. The simulated rays could undergo up to 8 reflections, 10 transmissions, and 2 diffractions. The computed PL values were measured in decibels (dB) and saved as grayscale `.png` images. The minimum and maximum PL values in the training dataset are 13 dB and 160 dB, respectively.

Each PL radio map is associated with an input RGB image (of the same length and width as the corresponding PL radio map) that conveys physical information about the propagation environment and the simulation of the PL values. Specifically, the 3 channels of the input image represent (i) the normal incidence reflectance of each material (zero for air), (ii) the normal incidence transmittance of each material (zero for air), and (iii) the physical distance from the Tx to each point of the grid. In addition, the coordinates of the Tx location are provided for each target radio map. Figure 1 illustrates a typical instance from the dataset, showing three input components and their corresponding ground truth.

2.2. Test Dataset

An additional test dataset, which had not been published before, was used to evaluate the performance of the submitted methods. The test dataset was generated through the same procedure used for the Indoor Radio Map Dataset. It involves five indoor geometries, one frequency band (868 MHz), and 25 or 50 transmitter (Tx) positions per indoor layout, resulting in a total of 200 radio maps.

Remark 2: *Note that we provided a training dataset with three center frequencies (868 MHz, 1.8 GHz, and 3.5 GHz, Task 2 sub-dataset of Indoor Radio Map Dataset), although the test dataset involved only one frequency (868 MH). The decision of how to use the training dataset was left up to the participants, i.e., they could use either the entire training sub-dataset or only the part that corresponds to the test frequency. Our rationale for doing this was twofold.* ***1)*** *In machine learning tasks, one frequently has access to training data from a setting that is analogous to the test setting, although they may not be a precise match. Nevertheless, their utilization may still yield favorable outcomes.* ***2)*** *The training dataset for the three center frequencies was already publicly available [12] and we wanted to provide a fair basis for comparison by informing all the participants of its availability. These additional data could prove useful, as detailed above and as evidenced by the fact that they were utilized by all the successful participating teams (cf. Sec. 5).*

3. THE COMPETITION TASKS

The competition consisted of two supervised learning tasks, Task 1 and Task 2, constituting 60% and 40% of the total score, respectively. Both tasks aimed to accurately and efficiently estimate PL radio maps of indoor environments.

[2] `https://www.ranplanwireless.com/`

$$\text{RMSE}^{t,r} = \sqrt{\frac{1}{\sum_{n\in\mathcal{D}} W_n H_n - |\mathcal{S}_n^{t,r}|} \sum_{n\in\mathcal{D}} \sum_{i=1}^{W_n} \sum_{j=1}^{H_n} \left(\mathbb{1}_{\{(i,j)\notin\mathcal{S}_n^{t,r}\}} \left(\tilde{\text{PL}}_n^{t,r}(i,j) - \text{PL}_n(i,j) \right) \right)^2} \tag{2}$$

For this purpose, participants used the provided input RGB image (cf. Sec. 2.1), which contains physical properties of the propagation scenario of interest, i.e., the electromagnetic properties of the walls, which implicitly also provides information about the building layout, along with sparse samples from the target (ground truth) PL radio map. For both tasks, two equally weighted sampling rates were considered: 0.5% and 0.02% of the total spatial points. This enabled investigating a high and a low sampling rate regime under different sampling strategies, resulting in a total of four sub-tasks.

Let $\mathcal{S}_n^{t,r}$ denote the sampling points for the n-th radio map with a sampling rate of r (in percent), for Task $t \in \{1, 2\}$. The number of sampling points were found by

$$|\mathcal{S}_n^{t,r}| = \lceil \frac{r W_n H_n}{100} \rceil, \tag{1}$$

where $\lceil \cdot \rceil$ denotes the ceiling function, and W_n and H_n are the width and length of the n-th radio map. As mentioned previously and detailed below in Sections 3.1 and 3.2, the Tasks differed in how the locations of $\mathcal{S}_n^{t,r}$ are determined.

The participants were permitted to employ the supplied ground truth PL samples in a flexible manner, provided that this did not lead to impractical computational times. Furthermore, the PL samples from a specific test radio map were to be utilized exclusively for the estimation of that radio map.

A key component of a successful submission was that the total run-time of a method should be significantly smaller than that of the underlying propagation model used to generate the ground truth dataset (i.e., Ranplan Wireless). Previous work in the literature, as well as the results of *The First Pathloss Radio Map Prediction Challenge* [9, 1], and *The First Indoor Pathloss Radio Map Prediction Challenge* [10], indicate that run-times on the order of 10–100 ms are reasonable on modern GPUs.

As mentioned previously, the radio maps (and their corresponding input images) in the Indoor Radio Map Dataset have varying lengths and widths. The participants were also tasked with addressing this issue. The common practice of resizing the images to a fixed resolution (as outlined in [4]) was communicated to the participants along with a script that performs this. Naturally, the performance metrics are still based on the degree of alignment with the original-size ground truth radio map images (cf. Sec. 4).

3.1. Task 1

For this Task, the locations of the sampling points of the n-th radio map were found by the organizers by uniformly randomly drawing $|\mathcal{S}_n^{t,r}|$ (cf. (1)) points without replacement from the total $W_n H_n$ points of the radio map. The 0.02% rate samples were selected as a subset of the 0.5% rate samples.

3.2. Task 2

Given the number of sampling points, the participants were asked to choose their own sampling points for this Task. The objective of this Task was to examine the merits of carefully selecting sampling points instead of using random sampling.

4. EVALUATION METHODOLOGY

To evaluate the fidelity of each submitted method for each sub-task, we computed the root mean square error (RMSE), excluding the sampling points of the ground truth samples used to aid the radio map reconstruction. Specifically, for each Task t and rate r, we computed the RMSE via (2), where $\mathbb{1}_{\{\cdot\}}$ is the indicator function, $\mathcal{D}$ denotes the test dataset, and $\tilde{\text{PL}}_n^{t,r}(i,j)$ and $\text{PL}_n(i,j)$ are the predicted and the ray tracing ground truth PL values in dB of the n-th radio map at pixel (i,j), respectively. The final score F was calculated as a weighted average of the RMSEs of the sub-tasks

$$\begin{aligned} \text{F} = 0.3 \times (\text{RMSE}^{1,0.02\%} + \text{RMSE}^{1,0.5\%}) + \\ 0.2 \times (\text{RMSE}^{2,0.02\%} + \text{RMSE}^{2,0.5\%}). \end{aligned} \tag{3}$$

5. SUBMITTED METHODS

Out of the eleven submissions, seven solutions demonstrated remarkable performance (cf. Table 1). We expound on these approaches in the following subsections.

5.1. Feng et al. [13]

SAIPP-Net is a UNet-based neural network that incorporates consecutive dilated convolution layers. It uses an augmented model channel input that improves upon the standard 3GPP InH model by incorporating a learnable material attenuation vector and a material count map. The authors assign higher sampling probabilities to regions farther from the transmitter and to those with larger signal gradients, estimated from an initial radio map. For the 0.02% sampling rate, they first pretrain a model without sampled values and then fine-tune it using the sparse samples. In contrast, for the 0.5% sampling rate, the sampled pathloss radio map is incorporated as an additional input channel to the DNN.

5.2. Xing et al. [14]

The authors use a UNet-based model and, in addition to standard input features, include several environment-aware geometric features such as obstruction count maps, accumulated transmittance maps, free-space pathloss, and log-scaled distance as additional input channels. Each input channel is individually normalized to ensure a consistent dynamic range across features. To handle varying propagation environment sizes, they apply dynamic padding at the batch level. They also employ a hybrid sampling strategy that allocates 95% of the sampling budget to uniform points and 5% to corner points, which are extracted using the Harris detector from the reflectance channel.

Table 1: Competition results showing the RMSEs (in dB) of the submitted methods on the test set for the case of no samples (ablation study), and for each sub-task, the final weighted RMSE, and the approximate run-time of each method (in milliseconds). **Row 1** presents the ablation study results, illustrating the impact of not using sparse ground truth samples as inputs. **Rows 2–5** show how the methods performed in each sub-task of the competition. **Row 6:** The final scores calculated as a weighted average of the RMSEs across these sub-tasks (3). **Row 7:** Rough average overall run-times (including pre-processing/fine-tuning) and inference times of the DNNs alone (in parentheses).

Team	Feng et al. [13]	Xing et al. [14]	Zheng et al. [15]	Chen et al. [16]	Petrosyan et al. [17]	TerRaIn [18]	Kojima et al. [19]	Javid et al.	Tang et al.	Ge et al.	UDENAR
Ablation (no samples) [dB]	6.90	11.17	7.00	6.42	6.85	6.71	16.08	N/A	N/A	N/A	N/A
Task 1 0.02% [dB]	**5.99**	6.12	6.36	6.20	6.42	6.91	7.63	7.76	7.75	9.97	11.35
Task 2 0.02% [dB]	6.08	6.84	6.27	**5.91**	6.54	6.91	7.78	7.93	10.70	7.97	11.28
Task 1 0.5% [dB]	3.32	**3.17**	3.57	4.36	4.01	4.18	4.50	8.33	7.76	8.45	5.77
Task 2 0.5% [dB]	3.28	**3.22**	3.52	3.84	3.65	3.81	4.51	8.11	7.69	6.95	7.30
Final (weighted) [dB]	**4.67**	**4.80**	**4.94**	**5.12**	**5.17**	**5.47**	**6.10**	8.04	8.33	8.51	8.85
Run-time (rough) [ms]	65 (6)	13.84 (1.27)	38.27 (34.22)	57.18 (48.92)	90.32 (7.90)	151.82 (142.72)	15,82 (4.48)	N/A	N/A	N/A	N/A

5.3. Zheng et al. [15]

The proposed model is built on a UNet encoder–decoder architecture and incorporates an enhanced Transformer module. The conventional fully connected linear layers in the self-attention and feed-forward modules within the Transformer are replaced with combinations of 1×1 pointwise convolutions and depthwise separable convolutions. The authors incorporate a gating mechanism that enables the network to adaptively weight the features extracted from the attention module, thus allowing it to handle complex and diverse spatial feature distributions. The authors employ a spatial structure-aware stratified sampling strategy that optimizes sampling point distribution.

5.4. Chen et al. [16]

IRM-Net is a UNet variant that replaces traditional convolutional layers with a cascaded combination of a Detail Enhancement Block and a Detail Enhancement Attention Block to enhance the extraction of localized, fine-grained features. Dense connections are integrated into both the encoder and decoder, and multi-level feature interaction pathways are constructed to improve multi-scale contextual awareness and mitigate information loss caused by downsampling and upsampling operations. A radio map based on free-space pathloss is used as an additional input feature. The authors propose a range-based sampling strategy prioritizing locations farther from the Tx.

5.5. Petrosyan et al. [17]

The authors use a UNet-based model featuring ResNet-34 encoder and Atrous Spatial Pyramid Pooling bottleneck and additional input features of free-space pathloss, cumulative transmittance losses, log-distance from the antenna, and a binary mask of padded pixels. Data augmentations include rotation, distance scaling, synthetic wall insertion, and flipping. Their distance-weighted sampling strategy sets probabilities inversely proportional to Tx distance while enforcing minimum separation constraints. A variable-number sampling method is adopted during training. This method allows for the use of a single model for all considered sampling rates and outperforms the use of separate models.

5.6. TerRaIn [18]

The authors use a UNet-based model featuring a shortcut pathway that connects the sample input channel to the later stages, along with double convolutions with residual connections and stacked dilated convolutions applied before each upsampling and downsampling step. For Task 2, a uniform grid sampling strategy that excludes points near the Tx is used at the high sampling rate, while at the low sampling rate, sampling is focused on regions with higher prediction errors, typically areas with strong reflection effects. Transmittance-spread and free-space pathloss are incorporated as additional input features, and random flips and rotations are performed for data augmentation.

5.7. Kojima et al. [19]

Sparse-Guided RadioUNet is a UNet-variant, which takes the sampling mask as input, along with the samples and the standard inputs, and uses instance normalization and Leaky ReLU activations throughout. The authors applied random rotations, flips, and crops of the inputs to augment the data. Inspired by the classical anisotropic Total Variation regularizer, they introduce a Spread Loss term that penalizes discontinuities, though it may occasionally oversmooth sharp transitions. Their sampling strategy prioritizes environment edges, shadow regions, and line-of-sight/non-line-of-sight transition areas while enforcing high separation between sampling locations.

6. RESULTS AND CONCLUSIONS

The results of the competition are presented in Table 1 in detail, while representative visual examples are shown in Fig. 2. We would like to note that the reported run-times are based on running the evaluation scripts of the participants (on an NVIDIA RTX A5000 GPU) and should be considered rough estimates, as they may not fully reflect the ultimate efficiency of the methods.

The results show that all of the participants' methods substantially benefited from samples at the high sampling rate. In contrast, for many methods, samples at the low sampling rate yielded only marginal improvements compared to the zero-sample baseline (see ablation study in Table 1). In some cases, such as in [18] and in the samples-as-input scenario of

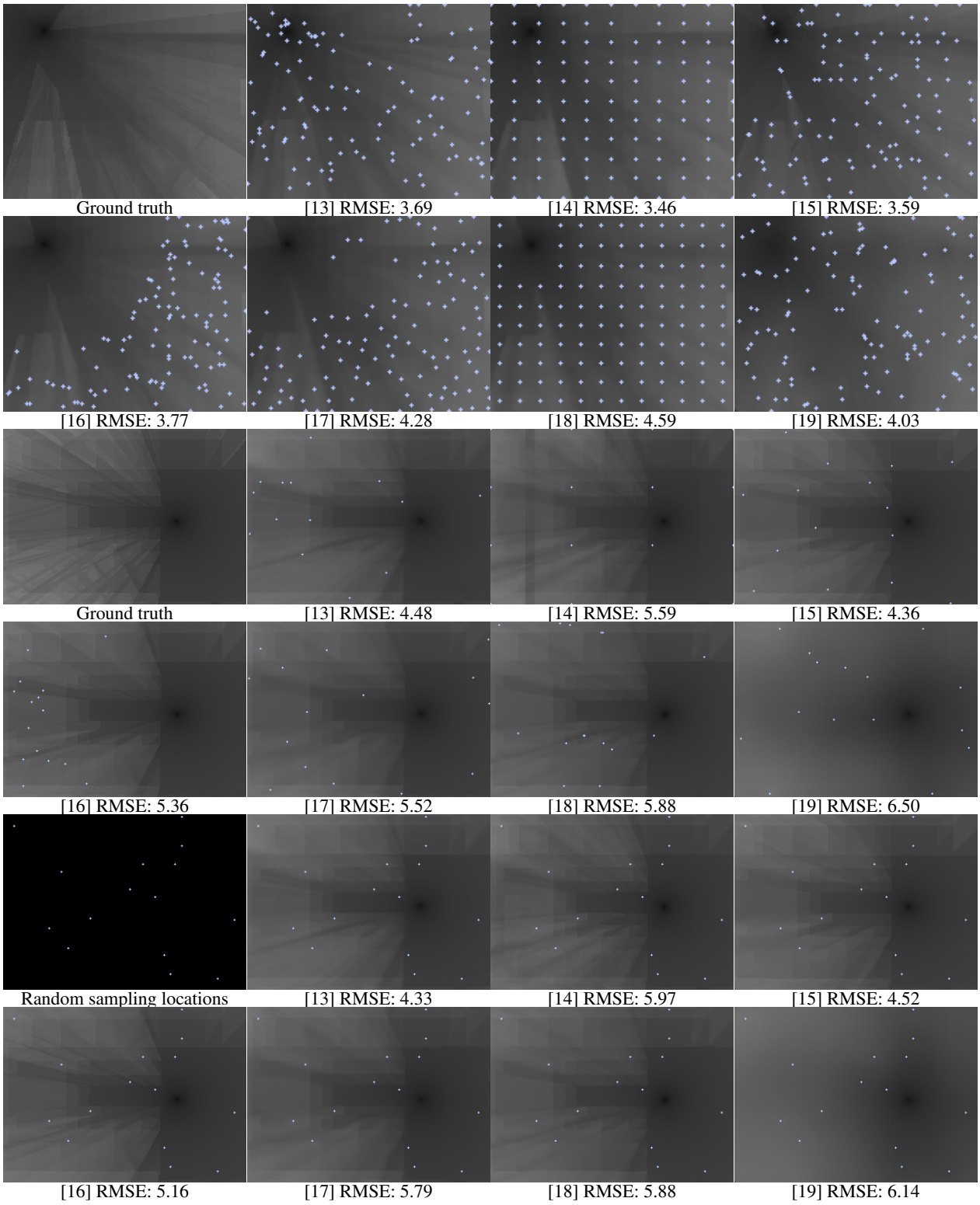

Fig. 2: Examples from the test dataset and participants' radio map estimates. The ground truth simulation and the radio map estimates of the successful seven participants are shown along with their per-image RMSEs. Sampling points are indicated by plus signs. **Rows 1-2:** An example from Building 4 (size 135 $\times$ 168) with sampling rate 0.5%, 114 sampling points chosen by the participants (Task 2). **Rows 3-4:** An example from Building 2 (size 230 $\times$ 319) with sampling rate 0.02%, 15 sampling points chosen by the participants (Task 2). **Rows 5-6:** The same example from Building 2 with sampling rate 0.02%, 15 samples. Each method was given the same samples, which were randomly selected by the organizers (Task 1).

[13], using low-rate samples even led to lower accuracy. Furthermore, the selective sampling strategies employed by participants generally did not produce consistent improvements over random sampling across the two sampling rates, with the exception of [15, 16]. We hope these general observations serve as a strong motivation for future research.

7. REFERENCES

[1] Ç. Yapar, F. Jaensch, R. Levie, G. Kutyniok, and G. Caire, "Overview of the first pathloss radio map prediction challenge," *IEEE Open Journal of Signal Processing*, pp. 1–16, 2024.

[2] S. Bakirtzis, Ç. Yapar, M. Fiore, J. Zhang, and I. Wassell, "Empowering wireless network applications with deep learning-based radio propagation models," *IEEE Wireless Communications*, pp. 1–8, 2025.

[3] R. Levie, Ç. Yapar, G. Kutyniok, and G. Caire, "RadioUNet: Fast radio map estimation with convolutional neural networks," *IEEE Transactions on Wireless Communications*, vol. 20, no. 6, pp. 4001–4015, 2021.

[4] S. Bakirtzis, J. Chen, K. Qiu, J. Zhang, and I. Wassell, "EM DeepRay: An expedient, generalizable, and realistic data-driven indoor propagation model," *IEEE Transactions on Antennas and Propagation*, vol. 70, no. 6, pp. 4140–4154, 2022.

[5] X. Zhang, X. Shu, B. Zhang, J. Ren, L. Zhou, and X. Chen, "Cellular network radio propagation modeling with deep convolutional neural networks," in *Proceedings of the 26th ACM SIGKDD International Conference on Knowledge Discovery & Data Mining*, New York, NY, USA, 2020, KDD '20, p. 2378–2386, Association for Computing Machinery.

[6] D. Romero and S.-J. Kim, "Radio map estimation: A data-driven approach to spectrum cartography," *IEEE Signal Processing Magazine*, vol. 39, no. 6, pp. 53–72, 2022.

[7] Y. Zeng, J. Chen, J. Xu, D. Wu, X. Xu, S. Jin, X. Gao, D. Gesbert, S. Cui, and R. Zhang, "A tutorial on environment-aware communications via channel knowledge map for 6G," *IEEE Communications Surveys Tutorials*, vol. 26, no. 3, pp. 1478–1519, 2024.

[8] B. Feng, M. Zheng, W. Liang, and L. Zhang, "A recent survey on radio map estimation methods for wireless networks," *Electronics*, vol. 14, no. 8, 2025.

[9] Ç. Yapar, F. Jaensch, R. Levie, G. Kutyniok, and G. Caire, "The first pathloss radio map prediction challenge," in *ICASSP 2023 - 2023 IEEE International Conference on Acoustics, Speech and Signal Processing (ICASSP)*, Rhodes, Greece, 2023, pp. 1–2.

[10] S. Bakirtzis, Ç. Yapar, K. Qiu, I. Wassell, and J. Zhang, "The first indoor pathloss radio map prediction challenge," in *ICASSP 2025 - 2025 IEEE International Conference on Acoustics, Speech and Signal Processing (ICASSP)*, Hyderabad, India, 2025, pp. 1–2.

[11] K. Qiu, S. Bakirtzis, I. Wassell, H. Song, K. Lin, and J. Zhang, "IRDM: A generative diffusion model for indoor radio map interpolation," in *GLOBECOM 2023-2023 IEEE Global Communications Conference*. IEEE, 2023, pp. 01–06.

[12] S. Bakirtzis, Ç. Yapar, K. Qui, I. Wassell, and J. Zhang, "Indoor radio map dataset," *IEEE Dataport*, 2024, `https://dx.doi.org/10.21227/c0ec-cw74`.

[13] B. Feng, M. Zheng, W. Liang, and L. Zhang, "SAIPP-Net: A sampling-assisted indoor pathloss prediction method for wireless communication systems," in *2025 IEEE 35th International Workshop on Machine Learning for Signal Processing (MLSP)*, Istanbul, Turkey, 2025.

[14] T. Xing, L. Zou, T. Bharadwaj, R. Balaji, and D. Cabric, "U-Net based indoor radio map prediction under sparse sampling," in *2025 IEEE 35th International Workshop on Machine Learning for Signal Processing (MLSP)*, Istanbul, Turkey, 2025.

[15] Z. Zheng, L. Xiao, M. Zhao, and Y. Li, "Efficient indoor radio map prediction with improved Transformers and active sampling strategies," in *2025 IEEE 35th International Workshop on Machine Learning for Signal Processing (MLSP)*, Istanbul, Turkey, 2025.

[16] Q. Chen, H. Tan, M. Yang, Jingjing Huang, and B. Chen, "IRM-Net: An enhanced attention networks for indoor radio map estimation," in *2025 IEEE 35th International Workshop on Machine Learning for Signal Processing (MLSP)*, Istanbul, Turkey, 2025.

[17] K. Petrosyan, H. Khachatrian, R. Mkrtchyan, and T. Raptis, "U-Net for indoor pathloss prediction from sparse measurements with physics-informed features," in *2025 IEEE 35th International Workshop on Machine Learning for Signal Processing (MLSP)*, Istanbul, Turkey, 2025.

[18] M. Wu, M. Skocaj, and M. Boban, "Radio map prediction via neural networks with ground truth shortcuts and selective sampling," in *2025 IEEE 35th International Workshop on Machine Learning for Signal Processing (MLSP)*, Istanbul, Turkey, 2025.

[19] R. Kojima, S. Ito, T. Nagao, and M. Taya, "Sparse-guided RadioUNet with adaptive sampling for the

MLSP 2025 sampling-assisted pathloss radio map prediction data competition," in *2025 IEEE 35th International Workshop on Machine Learning for Signal Processing (MLSP)*, Istanbul, Turkey, 2025.